Observing Dissipative Topological Defects with Coupled Lasers

Vishwa Pal,* Chene Tradonsky, Ronen Chriki, Asher A. Friesem, and Nir Davidson
Department of Physics of Complex Systems, Weizmann Institute of Science, Rehovot 7610001, Israel
(Received 3 February 2017; revised manuscript received 6 April 2017; published 7 July 2017)

Topological defects have been observed and studied in a wide range of systems, such as cosmology, spin systems, cold atoms, and optics, as they are quenched across a phase transition into an ordered state. These defects limit the coherence of the system and its ability to approach a fully ordered state, so revealing their origin and control is becoming an increasingly important field of research. We observe dissipative topological defects in a one-dimensional ring of phased-locked lasers, and show how their formation is related to the Kibble-Zurek mechanism and is governed in a universal manner by two competing time scales. The ratio between these two time scales depends on the system parameters, and thus offers the possibility of enabling the system to dissipate to a fully ordered, defect-free state that can be exploited for solving hard computational problems in various fields.

DOI: 10.1103/PhysRevLett.119.013902

Topological defects occur in various fields such as cosmology, spin systems, cold atoms, and optics, and continue to attract great attention [1–3]. Their origin and scaling behavior was first described by the Kibble-Zurek (KZ) mechanism as a continuous system is quenched across a phase transition into an ordered state via competing time scales [4–6]. The KZ mechanism was experimentally studied in various systems, such as atomic gases [7–9], nonlinear optics [10], and condensed matter systems [6,11]. Because of complexity and experimental limitations, these systems could not fulfill the exact KZ mechanism, and only deal with limited aspects [8,11–13]. Topologically protected defects may prevent the system from reaching a globally stable state with long range ordering [9]. In most of these works the phase transition into an ordered state was crossed by cooling the system from the outside. For the most interesting regime of fast cooling, it is hard to maintain uniformity over the entire system [7].

Here we present and characterize a new mechanism to form topological defects without external cooling in a dissipative system of coupled laser networks. In coupled lasers and polaritons, dissipative coupling can drive the system to a stable steady state phased-locked solution with minimal loss, which can be directly mapped to the ground state of the classical XY spin Hamiltonian [14–17]. However, when the dissipative dynamics is highly overdamped [18] and occurs on a complex landscape, the system fails to reach the globally stable solution and gets stuck in local minima. For a 1D system on a closed ring, such local minima are topological defects [9], characterized by a nonzero winding number (or topological charge) [19].

Topological defects have also been extensively studied in optical systems that involve continuous modes in multimode cavities (lasers or nonlinear mixers) where the coupling is mostly reactive [20–25]. We study such topological defects on a discrete 1D ring network of lasers with nearest neighbor dissipative coupling. Under the assumption of constant field amplitudes, such coupled lasers are well approximated as Kuramoto phase oscillators [18] that cannot unwind topological defects [26]. We show that fluctuations of the laser amplitudes, which are coupled to the laser phase dynamics, act as an effective temperature, and can unwind topological defects and anneal the system to a globally stable defect-free state. We also show that the formation of dissipative topological defects is connected to competition between internal and external time scales, and show the KZ mechanism in discrete systems with dissipative coupling. In laser networks, these competing time scales are the phase locking time [27,28] and synchronization time of the laser amplitude fluctuations [29–31]. Each time scale is controlled by many system parameters but the defect formation can be expressed by a single universal dependence on the ratio between them. Our approach to find the globally stable and minimum loss solution can be exploited for solving non-deterministic polynomial time hard problems (NP-hard problems) in various fields [15,32–34].

The network of lasers is formed in a degenerate cavity that consists of two cavity mirrors, a $4f$ telescope, a mask containing circular holes 10–30 in a ring geometry, and a Nd:YAG gain medium pumped by a 100 μs pulsed Xenon flash lamp [Fig. 1(a)]. The intracavity $4f$ telescope ensures that any field distribution at the mask plane is imaged onto itself after every round-trip. Accordingly, each hole on the mask corresponds to an independent individual laser [14,19,35,36]. We experimentally verified that lasers are independent, both in intensity and phase (i) by blocking one of the lasers inside the cavity and showing that intensities of other lasers are unaffected, and (ii) by showing that each laser is coherent with itself and incoherent with all the other lasers [37]. Coupling between adjacent lasers is introduced by moving the mirror M_1

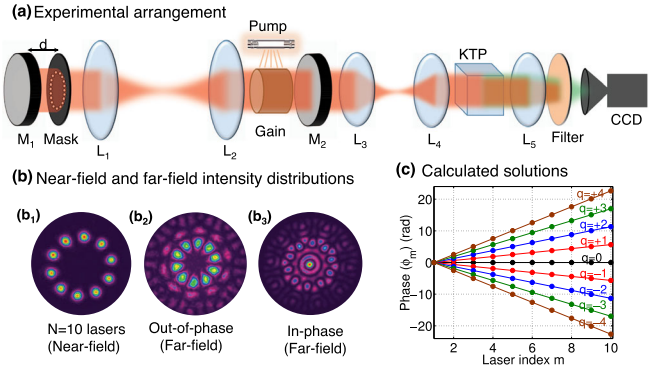

FIG. 1. Experimental arrangement with representative results. (a) Experimental arrangement; M_1 (high reflectivity) and M_2 (93% reflectivity) are cavity mirrors, L_1 and L_2 are plano-convex lenses in a $4f$ telescope configuration, L_3 and L_4 are plano-convex lenses in a demagnifying telescope configuration, KTP is a nonlinear crystal for SHG, L_5 is an imaging lens. The filter transmits only the frequency-doubled wavelength. (b) Representative experimental results for a ring network of 10 lasers: (b_1) near-field intensity distribution, (b_2) first harmonic far-field intensity distribution, and (b_3) second harmonic far-field intensity distribution. (c) Calculated steady-state solutions of a ring network 10 lasers for different topological charges $q = -4, -3, -2, -1, 0, +1, +2, +3, +4$.

away from the mask a distance (d) of a quarter-Talbot length [38], which provides negative coupling between the adjacent lasers, and results in a solution of out-of-phase ($0, \pi, 0, \pi, \ldots$) locked lasers [37,39]. The output from the lasers was then focused on to a nonlinear KTP crystal, so both the frequencies as well as the phases are doubled, and then imaged on a CCD camera. In such a second harmonic generation (SHG) scheme, the out-of-phase solution is converted into an in-phase solution (0, 0, 0, 0, ...), which is equivalent to phase locking of lasers with positive coupling [19,39].

Representative experimental results for phase locking 10 lasers on a ring network are shown in Fig. 1(b). The dark (bright) center in the first (second) harmonic far-field intensity distribution indicates out-of-phase (in-phase) locking [37].

While a continuous system can have a continuum of stable solutions, a discrete network has a finite number [40]. For example, as shown in Fig. 1(c), a ring of 10 coupled lasers has 9 steady-state solutions, where the phase of the laser m is $\phi_m = e^{iqm2\pi/10}$ and $q = -4, -3, \ldots, +4$ is the topological charge of each solution. The $q = 0$ in-phase solution is globally stable, whereas the eight $q \neq 0$ helical phase solutions are only locally stable. The dissipative coupling between lasers causes the system to converge to steady-state solutions with minimal loss [16]. Solutions with lower $|q|$ have lower losses, but this loss difference rapidly reduces with system size [26,37].

For ring networks of lasers to converge to a stable solution, all lasers must be phase locked and fulfill periodic boundary conditions. Yet, according to the Mermin-Wagner theorem long-range order cannot exist in one-dimensional systems in the thermodynamic limit [41]. Consequently, we limited our investigation to networks with $\leq$30 lasers, and ensured that all lasers are phase locked using a direct interference analysis [19,37].

To support and verify our experimental results, we numerically solved the rate equations that characterize a set of N single transverse and longitudinal modes class-B lasers, which are coupled linearly to each other [42], as

$$\frac{dA_m}{dt} = (G_m - \alpha_m)\frac{A_m}{\tau_p} + \sum_{n=(m)_{NN}} \frac{\kappa_{mn}}{\tau_p} A_n \cos(\phi_n - \phi_m), \quad (1)$$

$$\frac{d\phi_m}{dt} = \Omega_m + \sum_{n=(m)_{NN}} \frac{\kappa_{mn}}{\tau_p}\frac{A_n}{A_m}\sin(\phi_n - \phi_m), \quad (2)$$

$$\frac{dG_m}{dt} = \frac{1}{\tau_c}[P_m - G_m(|A_m|^2 + 1)], \quad (3)$$

where A_m, ϕ_m, G_m, α_m, Ω_m, and P_m are the amplitude, phase, gain, loss, frequency detuning, and pump strength of laser m, τ_p denotes the cavity round-trip time, τ_c the carrier lifetime, κ_{mn} the coupling coefficient between lasers m and n, and $n = (m)_{NN}$ the sum over laser m's NN (nearest neighbors) [43]. Coupling between higher order neighbor lasers were negligible in our system. The coupled equations [Eqs. (1)–(3)] were numerically solved with periodic boundary conditions using the fourth-order Runge-Kutta method, with our system parameters of $\tau_p = 5.4$ ns, $\tau_c = 230$ μs, and $\alpha_m = 0.1$. The distribution of detuning was $\Omega_m \ll \kappa_{mn}/\tau_p$, as provided by our degenerate cavity [14], ensuring that the coupling strength was well above the critical value [27,29]. The values of κ_{mn}, Ω_m, and P_m/P_{th} (P_{th} is the threshold pump strength) [37] in the simulation were determined by fitting to the experimental results.

If the amplitudes A_m of all lasers are equal, Eq. (2) reduces to the well-known Kuramoto equation of coupled phase oscillators [14,18] as

$$\frac{d\phi_m}{dt} = \Omega_m + \sum_{n=(m)_{NN}} \frac{\kappa_{mn}}{\tau_p}\sin(\phi_n - \phi_m). \quad (4)$$

The Kuramoto model was successfully applied in many areas such as populations of coupled oscillators [18], complex networks [44], and coupled laser arrays [45].

We quantified topological defects by analyzing the steady-state far-field intensity distributions measured after SHG, as described above. For 10 lasers [Figs. 2(a)–2(c)], the far-field intensity distribution has a clearly observable bright central peak and distinct dark and bright rings, indicating a nearly pure $q = 0$ in-phase solution. For 20 lasers [Figs. 2(d)–2(f)], the far-field intensity distribution has largely smeared dark and bright rings, manifesting the presence of topological defects [19]. Because of the

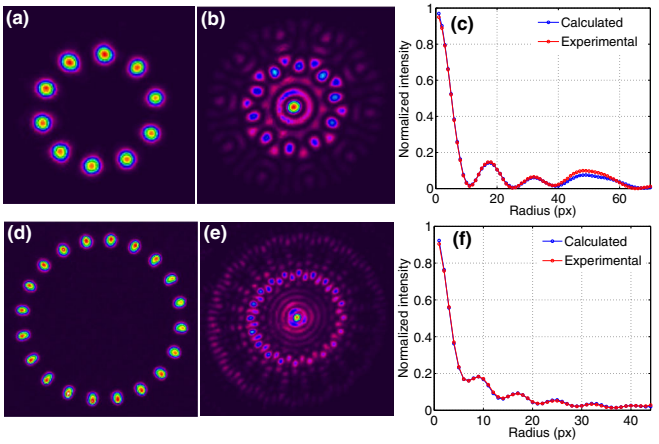

FIG. 2. Topological defects in ring networks of 10 (top row) and 20 (bottom row) lasers. (a),(d) Experimental near-field intensity distributions. (b),(e) Experimental far-field intensity distributions after SHG. (c),(f) Experimental and calculated radial intensity profiles of far-field intensity distributions after SHG. The probability of topological defects is found to be 2% for 10 lasers, and 18% for 20 lasers.

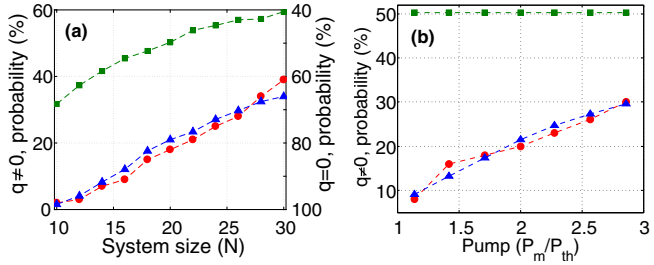

FIG. 3. Dissipative topological defects: (a) Probability of locally stable topological defects ($q \neq 0$) and globally stable in-phase solution ($q = 0$) as a function of system size. Red circles are experimental results; blue triangles are numerical results with full laser rate equations showing good agreement with the experimental result; green squares are numerical results with the Kuramoto model indicating much higher defect probability than in the experiment. (b) For a ring network of 20 lasers, the probability of topological defects as a function of normalized pump strength P_m/P_{th}. The simulated results of the laser rate equations are in good agreement with the experimental results while the Kuramoto model results predict much higher defect probability. The coupling strength in the simulation was $\kappa_{mn} = 0.01$.

multiplicity of longitudinal modes in each laser, each experimental realization corresponds to an ensemble average of many independent experiments, and directly provides the probability distribution of topological defects [14]. We thus determined the probability of topological defects by fitting the experimental radial intensity profiles with the calculated profiles [19,37]. For 10 lasers, we obtained 2% topological defects, whereas for 20 lasers, the topological defects increased to 18% [46]. We repeated this for various system sizes and the results are shown in Fig. 3(a) (red circles).

To support our experimental results, we first integrated the Kuramoto equation [Eq. (4)] with initial phases randomly distributed between 0 and 2π, until a steady state solution was reached and determined its q. We repeated this for 5000 different random initial phases, and determined the probability of globally stable ($q = 0$) and locally stable ($q \neq 0$) solutions. We found that the calculated probability of topological defects [green squares in Fig. 3(a)], is much larger than that obtained in the experiment [red circles in Fig. 3(a)], which demonstrates the inherent limitations of the Kuramoto model.

The large discrepancy between the Kuramoto and experimental results indicates that the coupled laser dynamics provides an additional mechanism to unwind a topological defect. To confirm and clarify such a mechanism, we resorted to the full laser rate equations [Eqs. (1)–(3)], which also take into account variations and fluctuations of the lasers amplitudes. For $P_m/P_{\mathrm{th}} = 14.2$ and $\kappa_{mn} = 0.01$, we obtained very good agreement between the simulated [blue triangles in Fig. 3(a)] and the experimental results. This suggests that laser amplitude dynamics indeed provide a mechanism to suppress topological defects.

Since the amplitude dynamics is directly related to pump strength [47], we also investigated the effect of pump strength P_m on the probability of topological defects in the steady state. The experimental results, presented in Fig. 3(b), are in good agreement with the simulated results of laser rate equations but not with the Kuramoto results.

The probability of topological defects increases with the pump strength and approaches the Kuramoto results for $P_m/P_{\mathrm{th}} \to \infty$, (when the Kuramoto assumption of uniform amplitudes is fulfilled [14,29]). Alternatively, as P_m approaches P_{th}, the effect of amplitude dynamics becomes more significant [47]. The probability of topological defects approaches zero and the system dissipates to the globally stable solution. This agrees with recent results of an OPO-based Ising machine [15], where P_m was shown to link to temperature [34]. The generation of vortices as a function of pump strength was also studied in a continuous system via bifurcation [25].

The control over topological defects by the pump strength and analogy with temperature can be put in the context of the KZ mechanism, where the density of defects scales with the cooling rate at which the phase transition is crossed [4,5]. In analogy to Zurek's approach, we identified two competing time scales in our system, namely, the synchronization time of laser amplitude fluctuations (t_{amp}) and the locking time of their phases (t_{phase}). The synchronization of intensity fluctuations in two coupled lasers was investigated in the past [30,31]. To evaluate how these two competing time scales depend on various laser parameters, we simulated the dynamical behaviors of the amplitudes and phases of the lasers using Eqs. (1)–(3).

The results of these simulations at two different pump strengths, for a system of $N = 20$ lasers, are shown in

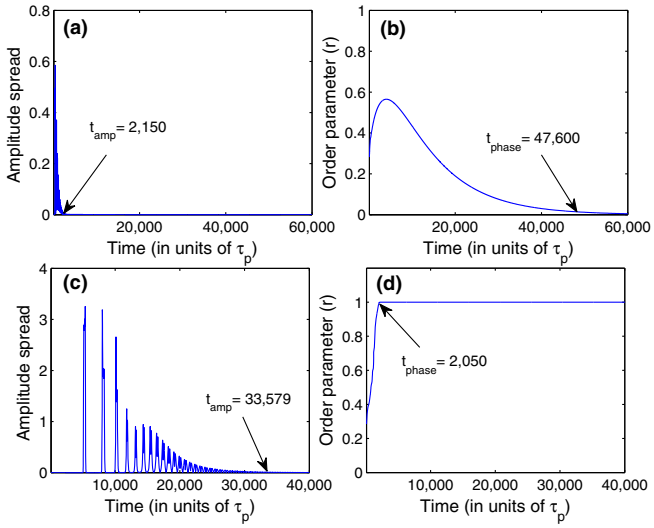

FIG. 4. Simulated dynamical behaviors of the laser amplitudes and phases at two different pump strengths, for a ring network of $N = 20$ lasers. The amplitude spread and phase order parameter are shown as a function of time for pump strength $P_m/P_{\mathrm{th}} = 16.7$ in (a) and (b), and for $P_m/P_{\mathrm{th}} = 1.25$ in (c) and (d) with the same initial conditions and coupling strength $\kappa = 0.001$. The arrows denote the amplitude synchronization time (t_{amp}) and phase locking time (t_{phase}). When $t_{\mathrm{amp}} \ll t_{\mathrm{phase}}$, the system is stuck in a locally stable state with $q \neq 0$ (top), and when $t_{\mathrm{amp}} > t_{\mathrm{phase}}$, the system reaches the globally stable state $q = 0$ state (bottom).

Fig. 4. Figures 4(a) and 4(c) show the amplitude dynamics, represented as normalized amplitude spread among the lasers $\sqrt{\langle (A_m - \langle A_m \rangle)^2 \rangle}/\langle A_m \rangle$, at $P_m/P_{\mathrm{th}} = 16.7$ and at $P_m/P_{\mathrm{th}} = 1.25$. As evident, the initial amplitude fluctuations decay much faster for high P_m/P_{th} [47]. In particular, the time t_{amp}, where the envelope of amplitude spread reaches 0.01 is ~15 times longer for low P_m/P_{th} [48]. Figures 4(b) and 4(d) show the phase locking dynamics, characterized by the order parameter $r(t) = |(1/N)\sum_{m=1}^{N} e^{i\phi_m(t)}|$ [18]. For high P_m/P_{th} phase locking is much slower than for low P_m/P_{th} and the t_{phase} [the time where $r(t)$ reaches within 0.01 of its steady state value] is ~23 times longer. In summary, at high P_m/P_{th}, $t_{\mathrm{amp}} \ll t_{\mathrm{phase}}$, whereas at low P_m/P_{th}, $t_{\mathrm{amp}} \gg t_{\mathrm{phase}}$.

The amplitude fluctuations can be regarded as an effective temperature [29] that is coupled to the phase dynamics [Eq. (2)] and the phase locking time t_{phase} corresponds to the information exchange time. Hence, for $t_{\mathrm{amp}} \ll t_{\mathrm{phase}}$, the external cooling rate is much faster than the internal information exchange rate, thereby promoting the generation of topological defects in accordance with the KZ mechanism. For $t_{\mathrm{amp}} \gg t_{\mathrm{phase}}$, the fluctuating amplitudes can "kick" the system out of the locally stable solutions, allowing it to find the globally stable solution.

To generalize the relation between topological defects and the competing time scales of the system, we also analyzed the probability of topological defects for different coupling strengths. For each coupling strength, we varied the pump

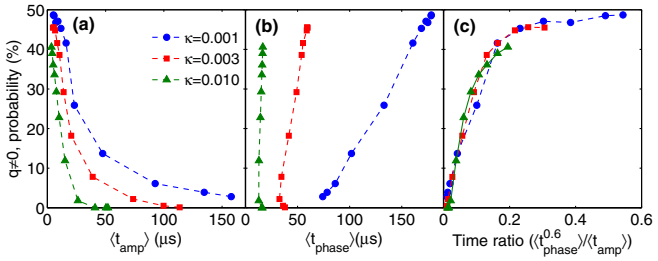

FIG. 5. Simulated probability of topological defects for a ring network of 20 lasers, using the laser rate equations, (a) as a function of synchronization time of the laser amplitude fluctuations at three different coupling strengths, (b) as a function of phase locking time at different coupling strengths, and (c) as a function of the ratio $\langle t_{\mathrm{phase}}^{0.6} \rangle / \langle t_{\mathrm{amp}} \rangle$. In all figures, for each coupling strength, every point on the curves corresponds to different pump strength. All trajectories collapse to a single curve, indicating universality in the system.

and calculated the two time scales $\langle t_{\mathrm{amp}} \rangle$ and $\langle t_{\mathrm{phase}} \rangle$, averaged over 1000 random initial conditions. The results are shown in Fig. 5. As evident, the probability of topological defects grows as $\langle t_{\mathrm{amp}} \rangle$ *decreases* [Fig. 5(a)] and as $\langle t_{\mathrm{phase}} \rangle$ *increases* [Fig. 5(b)]. Nevertheless, each of the two time scales depends on the system size. When the probability of topological defects is plotted as a function of $\langle t_{\mathrm{phase}}^{0.6} \rangle / \langle t_{\mathrm{amp}} \rangle$ all trajectories collapse to a single curve [Fig. 5(c)]. Such data collapse indicates universality in the system as in the KZ. The results in Figs. 5(a) and 5(b) are consistent with the trends reported earlier for small systems [30,31].

In conclusion, we investigated dissipative topological defects in 1D ring networks of lasers, and showed how they are linked to the KZ mechanism. The probability of topological defects increases with system size and pump strength. The formation of topological defects depends on two competing time scales, namely, phase locking time and the synchronization time of amplitude fluctuations, in agreement with the KZ mechanism. We observed universality in the system where the probability of topological defects depends only on a single parameter related to the ratio between the two competing time scales. As opposed to the KZ mechanism where the system is cooled by an external heat bath, in our ring networks of lasers the amplitude fluctuations act as an internal heat bath that is coupled to the phases. We demonstrated the inherent limitations of many models of coupled oscillators that take into account only the phase dynamics, widely used in various fields. Our findings are important to the emerging field of using coupled coherent oscillators to simulate quantum systems. Furthermore, we plan to extend our work to 2D discrete systems, and show closer analogy to the KZ mechanism.

The authors acknowledge partial support from the Minerva Foundation, United States-Israel Binational Science Foundation, and the Israeli Planning and Budgeting Committee Fellowship Program.

*Corresponding author.
vishwa.pal@weizmann.ac.il

[1] A. D. Campo and W. H. Zurek, Int. J. Mod. Phys. A **29**, 1430018 (2014).
[2] N. D. Mermin, Rev. Mod. Phys. **51**, 591 (1979).
[3] P. Coullet, L. Gil, and F. Rocca, Opt. Commun. **73**, 403 (1989).
[4] T. W. B. Kibble, J. Phys. A **9**, 1387 (1976).
[5] W. H. Zurek, Nature (London) **317**, 505 (1985).
[6] S. M. Griffin, M. Lilienblum, K. T. Delaney, Y. Kumagai, M. Fiebig, and N. A. Spaldin, Phys. Rev. X **2**, 041022 (2012).
[7] N. Navon, A. L. Gaunt, R. P. Smith, and Z. Hadzibabic, Science **347**, 167 (2015).
[8] L. E. Sadler, J. M. Higbie, S. R. Leslie, M. Vengalattore, and D. M. Stamper-Kurn, Nature (London) **443**, 312 (2006).
[9] L. Corman, L. Chomaz, T. Bienaimé, R. Desbuquois, C. Weitenberg, S. Nascimbène, J. Dalibard, and J. Beugnon, Phys. Rev. Lett. **113**, 135302 (2014).
[10] S. Ducci, P. L. Ramazza, W. González-Viñas, and F. T. Arecchi, Phys. Rev. Lett. **83**, 5210 (1999).
[11] R. Monaco, J. Mygind, R. J. Rivers, and V. P. Koshelets, Phys. Rev. B **80**, 180501R (2009).
[12] P. C. Hendry, N. S. Lawson, R. A. M. Lee, P. V. E. McClintock, and C. D. H. Williams, Nature (London) **368**, 315 (1994).
[13] M. E. Dodd, P. C. Hendry, N. S. Lawson, P. V. E. McClintock, and C. D. H. Williams, Phys. Rev. Lett. **81**, 3703 (1998).
[14] M. Nixon, E. Ronen, A. A. Friesem, and N. Davidson, Phys. Rev. Lett. **110**, 184102 (2013).
[15] A. Marandi, Z. Wang, K. Takata, R. L. Byer, and Y. Yamamoto, Nat. Photonics **8**, 937 (2014).
[16] V. Eckhouse, M. Fridman, N. Davidson, and A. A. Friesem, Phys. Rev. Lett. **100**, 024102 (2008).
[17] N. G. Berloff, K. Kalinin, M. Silva, W. Langbein, and P. G. Lagoudakis, arXiv:1607.06065.
[18] J. A. Acebrón, L. L. Bonilla, C. J. P. Vicente, F. Ritort, and R. Spigler, Rev. Mod. Phys. **77**, 137 (2005).
[19] V. Pal, C. Trandonsky, R. Chriki, G. Barach, A. A. Friesem, and N. Davidson, Opt. Express **23**, 13041 (2015).
[20] E. J. D'Angelo, C. Green, J. R. Tredicce, N. B. Abraham, S. Balle, Z. Chen, and G. L. Oppo, Physica (Amsterdam) **61D**, 6 (1992).
[21] F. T. Arecchi, G. Giacomelli, P. L. Ramazza, and S. Residori, Phys. Rev. Lett. **67**, 3749 (1991).
[22] M. Brambilla, L. A. Lugiato, V. Penna, F. Prati, C. Tamm, and C. O. Weiss, Phys. Rev. A **43**, 5114 (1991).
[23] F. T. Arecchi, S. Boccaletti, P. L. Ramazza, and S. Residori, Phys. Rev. Lett. **70**, 2277 (1993).
[24] G. Huyet, M. C. Martinoni, J. R. Tredicce, and S. Rica, Phys. Rev. Lett. **75**, 4027 (1995).
[25] P. Genevet, S. Barland, M. Giudici, and J. R. Tredicce, Phys. Rev. Lett. **104**, 223902 (2010).
[26] D. A. Wiley, S. H. Strogatz, and M. Girvan, Chaos **16**, 015103 (2006).
[27] L. Fabiny, P. Colet, R. Roy, and D. Lenstra, Phys. Rev. A **47**, 4287 (1993).
[28] H. G. Winful, S. Allen, and L. Rahman, Opt. Lett. **18**, 1810 (1993).
[29] M. Nixon, M. Fridman, A. A. Friesem, and N. Davidson, Opt. Lett. **36**, 1320 (2011).
[30] V. Eckhouse, M. Nixon, M. Fridman, A. A. Friesem, and N. Davidson, IEEE J. Quantum Electron. **46**, 1821 (2010).
[31] I. Kanter, N. Gross, E. Klein, E. Kopelowitz, P. Yoskovits, L. Khaykovich, W. Kinzel, and M. Rosenbluh, Phys. Rev. Lett. **98**, 154101 (2007).
[32] M. Nixon, O. Katz, E. Small, Y. Bromberg, A. A. Friesem, Y. Silberberg, and N. Davidson, Nat. Photonics **7**, 919 (2013).
[33] C. H. Papadimitriou and K. Steiglits, *Combinatorial Optimization: Algorithims and Complexity* (Dover Publications, New York, 1998).
[34] T. Inagaki, K. Inaba, R. Hamerly, K. Inoue, Y. Yamamoto, and H. Takesue, Nat. Photonics **10**, 415 (2016).
[35] M. Nixon, M. Friedman, E. Ronen, A. A. Friesem, N. Davidson, and I. Kanter, Phys. Rev. Lett. **106**, 223901 (2011).
[36] M. Nixon, M. Friedman, E. Ronen, A. A. Friesem, N. Davidson, and I. Kanter, Phys. Rev. Lett. **108**, 214101 (2012).
[37] See Supplemental Material at http://link.aps.org/supplemental/10.1103/PhysRevLett.119.013902 for additional technical details, experimental, and calculated results.
[38] D. Mehuys, W. Streifer, R. G. Waarts, and D. F. Welch, Opt. Lett. **16**, 823 (1991).
[39] C. Tradosnky, M. Nixon, E. Ronen, V. Pal, R. Chriki, A. A. Friesem, and N. Davidson, Photon. Res. **3**, 77 (2015).
[40] C. N. Alexeyev, A. V. Volyar, and M. A. Yavorsky, Phys. Rev. A **80**, 063821 (2009).
[41] S. H. Strogatz and R. E. Mirollo, J. Phys. A **21**, L699 (1988).
[42] F. Rogister, K. S. Thornburg, L. Fabiny, M. Möller, and R. Roy, Phys. Rev. Lett. **92**, 093905 (2004).
[43] E. Ronen and A. A. Ishaaya, IEEE J. Quantum Electron. **47**, 1526 (2011).
[44] S. H. Strogatz, Nature (London) **410**, 268 (2001).
[45] G. Kozyreff, A. G. Vladimirov, and P. Mandel, Phys. Rev. Lett. **85**, 3809 (2000).
[46] For 10 lasers, the best fitting is achieved by superposition of 98% ($q = 0$) +2% ($|q| = 1$). Whereas, for 20 lasers, the best fitting is achieved by superposition of 82% ($q = 0$) +15% ($|q| = 1$) +3% ($|q| = 2$).
[47] A. Siegman, *Lasers* (University Science Books, Mill Valley, CA, 1986).
[48] We verified that using other criteria (e.g., within 10% of its steady state values) gives very similar results.